Design and Optimization of Propulsion Systems Employing Scarfed Nozzles

J. S. Lilley*
U.S. Army Missile Command, Redstone Arsenal, Alabama

A methodology for the design and optimization of tactical solid propellant propulsion systems employing scarfed nozzles is presented. A performance prediction computer code based on an axisymmetric flowfield model and utilizing the method-of-characteristics solution technique is employed as the primary analysis tool. This performance code is used through a series of parametric studies to obtain a performance map for length-constrained scarfed nozzles. The results of these parametric studies are curve-fitted to relationships that express scarf-nozzle performance as a function of nozzle geometric parameters. The relationships are differentiated to obtain the set of geometric parameters for a given nozzle projected length, which maximizes the motor axial performance. The set of optimum geometric parameters for each given nozzle projected length is employed in additional curve fits. These curve fits are used to express the optimum values of the geometric parameters and the corresponding optimum performance as a function of nozzle projected length. The curve fits for the optimum quantities are used to develop a series of relationships that expresses the length of a tactical propulsion system as a function of projected nozzle length. These system relationships are employed to obtain the nozzle geometry, which minimizes the propulsion system length for a specific delivered impulse requirement. The results of this study provide the propulsion system designer with a methodology for selecting the optimum nozzle design for length-constrained applications.

Nomenclature

A = area coefficient for optimum nozzle geometry curve fits
a = aft dome major radius
A_1-A_{20} = coefficients for optimum nozzle geometry curve fits
B = coefficient for optimum nozzle geometry curve fits
b = aft dome minor radius
C = coefficient for optimum nozzle geometry curve fits
C_F = thrust coefficient
C^* = characteristic velocity
D = coefficient for optimum nozzle geometry curve fits, motor case diameter
E = coefficient for optimum nozzle geometry curve fits
F = thrust
g = English units conversion factor
H_N = nozzle projected height
I_{sp} = specific impulse
I_{tot} = total impulse
K_N = ratio of burning surface area to throat area
L = length
L_N = nozzle projected length
$\dot{m}$ = mass flow rate
N_N = number of nozzles
P = pressure
P_r = perimeter of burning surface
R = ideal gas constant
R^2 = correlation coefficient
r_b = burning rate
r_t = throat radius
T = temperature
t_b = burn time
X = motor axial coordinate
X_1-X_3 = independent variables for nozzle performance curve fits
X_P = nondimensional nozzle projected length
x = nozzle axial coordinate
Y = motor radial coordinate, dependent variable for curve fits
Y_p = nondimensional nozzle projected height
y = nozzle radial coordinate
α = half-angle of basic nozzle
β = scarf angle
γ = specific heat ratio
ΔL_g = difference in grain length from reference grain
δ = half-angle of scarfed extension
ϵ = expansion ratio of basic nozzle
η = impulse efficiency
θ = cant angle
ρ_p = propellant density
ρ_{td} = downstream throat radius
ρ_{tu} = upstream throat radius

Subscripts

a = atmospheric
b = burning surface
c = combustion chamber, stagnation
cr = cross section
D = dome
del = delivered
g = grain
max = maximum
opt = optimum nozzle geometry
ps = propulsion system
ref = reference
t = throat
X = motor axial coordinate
x = nozzle axial coordinate
Y = motor radial coordinate
y = nozzle radial coordinate

Presented as Paper 85-1308 at the AIAA/SAE/ASME/ASEE 21st Joint Propulsion Conference, Monterey, CA, July 8-10, 1985; received Aug. 26, 1985; revision received Feb. 26, 1986.

*Aerospace Engineer, Propulsion Directorate. Member AIAA.

Introduction

TRADITIONALLY, the extreme aft section of a missile has been dedicated to the propulsion system. As a general rule, the rocket motor and nozzle system are located in the rear of the missile with the axis of the nozzle system oriented along the missile centerline. However, the guidance

requirements of several existing and proposed tactical missiles necessitate the location of guidance and control equipment in the aft region of the missile. In particular, the aft region of the missile has been considered an attractive location for equipment associated with the guidance link, e.g., actuators, receivers, or wire reels. Therefore, with these demands on the rear of the missile, there is a definite need in some tactical missile systems to move the propulsion system forward.

Locating the propulsion system in the midsection of the missile creates obvious problems. The nozzle system can no longer be on the missile axis. Instead, the nozzles employed must be canted at an angle to the missile centerline and exhaust out the side of the missile body. In addition, for aerodynamic purposes, these nozzles are truncated so that their exit planes are flush with the outer surface of the missile. Such nozzles are called "scarfed nozzles." An illustration of a typical scarfed-nozzle configuration is shown in Fig. 1. Due to the unconventional geometry of scarfed nozzles, the analysis methods and design rules that apply to axisymmetric nozzles are not generally applicable to scarfed nozzles. Therefore, it is apparent that methods for evaluating the performance of systems employing scarfed nozzles are required.

The purpose of the present investigation[1] is to address this need for scarfed-nozzle analysis methods. In particular, the intention was to develop a methodology with which scarfed nozzles could be designed. In conducting this investigation, the primary analysis tool was a performance prediction model which was extensively used and experimentally validated in previous investigations.[2,3] Using this model, a series of parametric studies was performed. The results of the parametric studies were incorporated into a design methodology. Using this methodology, optimum scarfed-nozzle designs can be obtained.

Performance Prediction Model

In order to investigate the performance of scarfed nozzles, an accurate performance prediction model is required. The performance model selected for the present investigation was a computer code developed by Hoffman.[4] This code is based on a two-dimensional axisymmetric flowfield model and uses the method-of-characteristics solution technique. The code is used to generate a flowfield solution and a performance prediction for a single scarfed-nozzle design. The following quantities are generated by the performance model:

F_x = thrust component along the nozzle axis
F_y = thrust component normal to the nozzle axis
F_X = thrust component along the missile axis
F_Y = thrust component normal to the missile axis
$\dot{m}$ = mass flow rate

The following relationships exist between thrust components measured relative to the missile axis and those measured relative to the nozzle axis.

$$F_X = F_x \cos\theta - F_y \sin\theta \tag{1}$$

$$F_y = F_x \sin\theta + F_y \cos\theta \tag{2}$$

where θ is the nozzle cant angle.

Additional performance factors can be generated from the values previously described. The value for motor axial specific impulse $I_{sp,X}$ is given by

$$I_{sp,X} = F_X/\dot{m} \tag{3}$$

The motor axial thrust coefficient $C_{F,X}$ is given by

$$C_{F,X} = F_X/(A_t P_c) \tag{4}$$

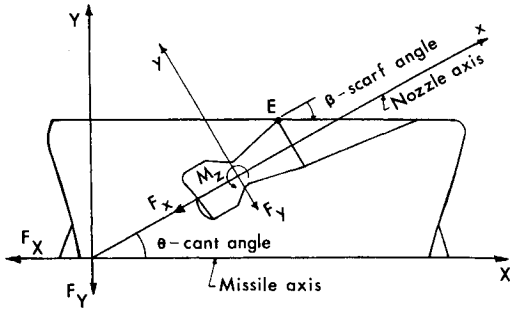

Fig. 1 Side-exiting scarfed propulsive nozzle.

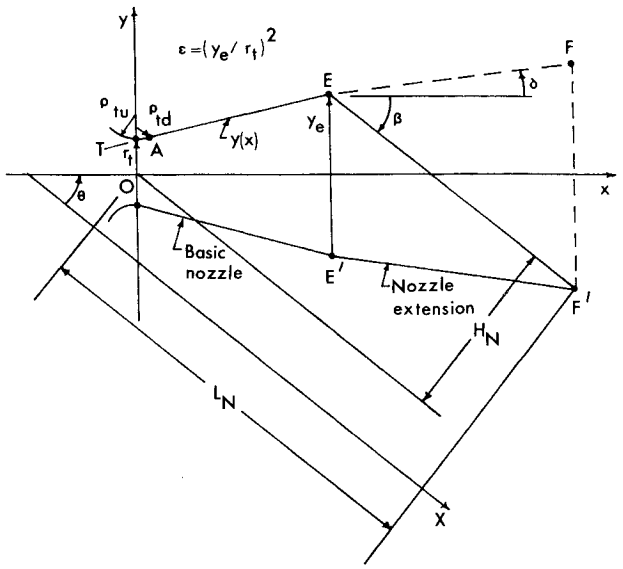

Fig. 2 Scarfed-nozzle geometric model.

where A_t is the total throat area of the nozzle. The characteristic velocity C^* is given by

$$C^* = (gA_tP_c)/\dot{m} \tag{5}$$

This code has been extensively employed as an analysis tool in previous investigations.[2,3]

Length-Constrained Scarfed Nozzles

The primary objective in considering the performance of scarfed nozzles is to evaluate performance in the context of a complete missile system. A common application of rocket motors employing scarfed nozzles is in small tactical missiles. Typically, such missiles have severe constraints placed on their physical dimensions. Quite often, upper limits are placed on the length and diameter of the missile. To accommodate these constraints, limitations are placed on the propulsion system. Typically, the propulsion system is required to deliver a specified total impulse over the course of the mission and fit within a maximum allowable diameter and length.

The length of a rocket motor is directly influenced by the performance of the nozzles employed. In particular, the specific impulse of the nozzles has a direct impact on the propulsion system length. The higher the delivered specific impulse the less propellant that is required, and thus the shorter the propellant length. However, the results of previous investigations[2,3] showed that, for scarfed nozzles, the highest motor axial specific impulse was achieved with nozzles that had large expansion ratios, small cant angles, and small nozzle half-angles. In general, such nozzles are quite long. Thus, it becomes evident that maximizing specific impulse will not

necessarily minimize motor length. Therefore, tradeoffs must be made between nozzle length and specific impulse. Thus, it is necessary to consider the performance of such nozzles in terms of nozzle length.

Nozzle Geometric Model

Presented in Fig. 2 is a meridional plane view of the geometric model. The basic nozzle consists of a double circular-arc throat contour joined smoothly to a conical supersonic expansion contour. The nozzle extension consists of a conical section beginning at the end of the basic nozzle. The cant angle θ is the angle between the nozzle and missile axes. In the present analysis, the cant angle is equal to the scarf angle β.

The throat geometry is completely specified by the throat radius r_t, the throat upstream and downstream radii of curvature ρ_{tu} and ρ_{td}, respectively, and the cone angle α, at which the supersonic expansion contour attaches smoothly to the circular-arc throat contour. The basic nozzle contour is specified by the cone angle α and area ratio ϵ. The geometry of the nozzle extension is completely specified by the angle δ of the conical extension and the scarf angle β. Therefore, the major independent design parameters for a scarfed nozzle, using the present geometry model, are α, β, ϵ, and δ. However, in order to consider system performance in terms of nozzle length, a different set of independent design variables must be applied. Instead of expansion ratio ϵ, some measure of nozzle length must be considered. The required variable is the projected length of the nozzle along the motor axis of symmetry measured from the center of the throat of the nozzle. This variable, denoted as L_N, along with the nozzle projected height H_N is illustrated in Fig. 2. The nondimensional representation of these values is given by

$$X_p = L_N / r_t \tag{6}$$

$$Y_p = H_N / r_t \tag{7}$$

Therefore, the nozzle design parameters to be considered are α, β, δ, and X_p.

Results of Previous Investigations

As a result of previous investigations, several significant findings were obtained concerning scarfed-nozzle performance.[2,3] These findings are directly applicable to all of the results presented in the subsequent sections.

The following statements can be made about the performance of scarfed nozzles.

1) If the scarf angle of the nozzle exceeds the local Mach angle throughout the scarfed extension, the flowfield in the extension will be axisymmetric.

2) The motor axial specific impulse, thrust coefficient, and thrust are independent of ambient pressure P_a.

3) The motor axial specific impulse and thrust coefficient are independent of stagnation pressure P_c.

4) The motor axial thrust is directly proportional to stagnation pressure P_c.

5) The motor axial specific impulse is only a function of nozzle geometry, stagnation temperature T_c, gas constant R, and specific heat ratio γ.

6) The motor axial thrust coefficient is only a function of motor geometry and specific heat ratio γ.

7) The motor axial thrust is only a function of motor geometry, stagnation pressure P_c, and specific heat ratio γ.

8) The motor axial specific impulse can be corrected to yield the performance of a given nozzle for any propellant with a specified value of γ. This relationship is as follows:

$$I_{sp,X_2} = \frac{C_2^*}{C_1^*} I_{sp,X_1} \tag{8}$$

where the subscripts 1 and 2 denote different propellants with the same value of γ.

The following additional statements can be made about the influence of geometry on the performance of unconstrained scarfed nozzles.

1) Motor axial specific impulse decreases slightly as cone angle α increases.

2) Motor axial specific impulse increases significantly as the area ratio ϵ increases.

3) Motor axial specific impulse increases slightly as cone angle δ increases.

4) Motor axial specific impulse decreases significantly as scarf angle β increases.

It should be noted that these and the previous findings are based on two major assumptions: the pressure level in the scarfed extension is sufficient to prevent flowfield separation, and the nozzle exit plane is flush with the missile skin ($\theta = \beta$).

Parametric Studies

In order to determine the influence of motor length on scarfed-nozzle performance, parametric studies were performed. During these studies, it was decided that the value of δ was not actually a free variable. For a practical nozzle, only two possible values of δ should be considered: $\delta = 0$ deg, where the scarfed extension is a cylindrical supersonic blast tube; and $\delta = \alpha$, where the scarfed nozzle is a truncated conical nozzle. As a result, two parametric studies were performed, one for each of the options for δ.

Table 1 presents the basic set of performance model inputs for these studies.

In these parametric studies, the independent variables considered were α, β, and X_p, with all other inputs considered as fixed. The dependent variable was chosen to be motor axial specific impulse, $I_{sp,X}$. For the case of $\delta = 0$ deg, the following set of independent variables was evaluated: $\alpha = 10$, 15, 20, 25, 30 deg; $\beta = 10$, 15, 20, 25, 30, 35, 40 deg; $X_p = 10$, 15, 20, 25, 30, 35, 40, 45, 50; with the restriction $\epsilon > 1.0$. For the case of $\delta = \alpha$, the following set of independent variables

Table 1

Geometric inputs	
r_t, in.	1.0
ρ_{tu}, in.	1.0
ρ_{td}, in.	0.01
Thermodynamic inputs	
P_c, psia	1000
P_a, psia	14.696
T_c, °R	5000
R, ft-lbf/(lbm-°R)	65
γ	1.2

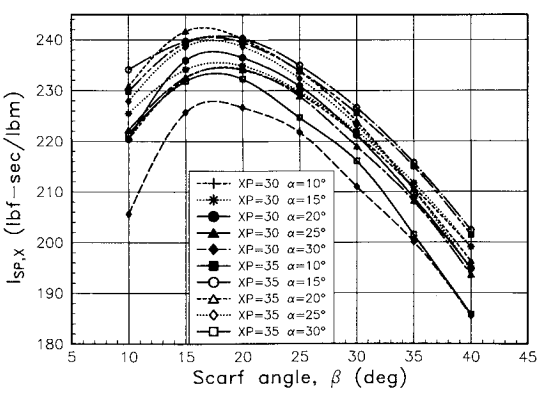

Fig. 3 Specific impulse as a function of scarf angle for $X_P = 30$, 35, and $\delta = 0$.

was evaluated: $\alpha = 5$, 10, 15, 20, 25, 30 deg; $\beta = 10$, 15, 20, 25, 30, 35, 40 deg; $X_p = 10$, 15, 20, 25, 30, 35, 40, 45, 50; with the restrictions $\epsilon > 1.0$ and $\beta > \alpha$.

The performance of the nozzles resulting from all possible combinations of the independent variables for each δ option was evaluated using the performance model. Representative results of the parametric study are presented graphically in Fig. 3 for the case of $\delta = 0$ deg, and in Fig. 4 for the case of $\delta = \alpha$.

Curve Fits

From the results presented in Figs. 3 and 4, it is evident that for each of the two parametric studies, for a given value of X_p, there must exist an optimum α and β combination, which produces the maximum specific impulse. The problem, therefore, is to find a means to accurately specify the geometry of these optimum nozzles. In order to obtain the optimum geometries from the results of the parametric studies, a means of translating the data points into smooth analytical surfaces was required. This was accomplished by performing a third-order least-squares curve fit on the results of each of the parametric studies. The general form of the curve fit is as follows:

$$\begin{aligned} Y = {} & A_1 + A_2X_1 + A_3X_2 + A_4X_3 + A_5X_1^2 + A_6X_2^2 + A_7X_3^2 \\ & + A_8X_1^3 + A_9X_2^3 + A_{10}X_3^3 + A_{11}X_1X_2 + A_{12}X_2X_3 \\ & + A_{13}X_3X_1 + A_{14}X_1^2X_2 + A_{15}X_1^2X_3 + A_{16}X_2^2X_1 \\ & + A_{17}X_2^2X_3 + A_{18}X_3^2X_1 + A_{19}X_3^2X_2 + A_{20}X_1X_2X_3 \end{aligned} \tag{9}$$

where

$$Y = C_{F,X} \tag{10}$$

$$X_1 = X_p \tag{11}$$

$$X_2 = \beta \text{ (deg)} \tag{12}$$

$$X_3 = \alpha \text{ (deg)} \tag{13}$$

To convert the specific impulse values to thrust coefficient values for use in the curve fit, the following relationship was used:

$$C_{F,X} = gI_{sp,X}/C^* \tag{14}$$

where $C^* = 5036.48$ ft/s. Thus,

$$C_{F,X} = [6.388193 \times 10^{-3} \text{lbm/(lbf-s)}]\, I_{sp,X} \tag{15}$$

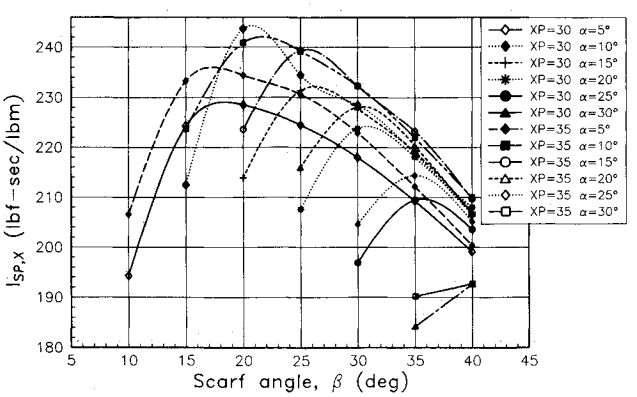

Fig. 4 Specific impulse as a function of scarf angle for $X_p = 30$, 35, and $\delta = \alpha$.

The coefficients for these curve fits are presented in Table 2.

Nozzle Performance Optimization

With the scarfed-nozzle performance results from the parametric studies curve-fitted, the optimum geometries that result from those curve fits can be determined. From each curve fit, it is desired to find the geometry that produces the maximum thrust coefficient for a given nozzle length. The curve fits used are a function of the following form:

$$C_{F,X} = C_{F,X}(X_p, \beta, \alpha) \tag{16}$$

Thus, for a fixed value of X_p, the maximum value of $C_{F,X}$ must occur at the following point:

$$\frac{\partial C_{F,X}}{\partial \beta} = \frac{\partial C_{F,X}}{\partial \alpha} = 0 \tag{17}$$

Applying this relationship to Eq. (9) yields the following two simultaneous equations:

$$\begin{aligned} & A_3 + 2A_6X_2 + 3A_9X_2^2 + A_{11}X_1 + A_{12}X_3 + A_{14}X_1^2 \\ & \quad + 2A_{16}X_2X_1 + 2A_{17}X_2X_3 + A_{19}X_3^2 + A_{20}X_1X_3 = 0 \end{aligned} \tag{18}$$

$$\begin{aligned} & A_4 + 2A_7X_3 + 3A_{10}X_3^2 + A_{12}X_2 + A_{13}X_1 + A_{15}X_1^2 \\ & \quad + A_{17}X_2^2 + 2A_{18}X_3X_1 + 2A_{19}X_3X_2 + A_{20}X_1X_2 = 0 \end{aligned} \tag{19}$$

For a given value of X_p, these two equations can be used to solve for the optimum values of α and β. An iterative technique was applied to obtain solutions to the preceding system of equations. For both curve fits, the solutions for the optimum geometries were obtained for values of X_p from 10 to 50. The optimum values of α, β, ϵ, Y_p, and $C_{F,X}$ for both curve fits are presented graphically as functions of X_p in Figs. 5-9, respectively. The results presented in Figs. 5-9 were curve-fitted with a fourth-order polynomial of the following form:

$$Y = AX_p^4 + BX_p^3 + CX_p^2 + DX_p + E \tag{20}$$

where $Y = \alpha$, β, ϵ, Y_p, or $C_{F,X}$. The results of these curve fits are presented in Table 3.

Table 2 Results of thrust coefficient curve fits[a]

	$\delta = 0$ deg	$\delta = \alpha$
A_1	−0.4379586E+00	−0.5094662E+00
A_2	0.8032080E−01	0.5731287E−01
A_3	0.1016197E+00	0.1305920E−00
A_4	−0.5300941E−02	−0.4478513E−01
A_5	−0.1311598E−02	−0.7644726E−03
A_6	−0.2686483E−02	−0.4427299E−02
A_7	−0.4706413E−03	−0.4763003E−02
A_8	0.7073229E−05	0.4207677E−03
A_9	0.2258740E−04	0.4788766E−04
A_{10}	−0.1013209E−04	−0.4091555E−05
A_{11}	−0.1947016E−02	−0.1350872E−02
A_{12}	0.9157079E−03	0.6157818E−02
A_{13}	0.5257240E−03	0.7442523E−03
A_{14}	0.1633709E−04	0.5865543E−05
A_{15}	−0.5279598E−05	−0.3425468E−05
A_{16}	0.1736288E−04	0.1630361E−04
A_{17}	−0.1414855E−04	−0.1071218E−03
A_{18}	0.1032215E−04	0.1790339E−04
A_{19}	0.1219364E−04	0.9758366E−04
A_{20}	−0.1972002E−04	−0.2963217E−04

[a]No. of points: $\delta = 0$ deg, 373; $\delta = \alpha$, 234. Correlation coefficient R^2: $\delta = 0$ deg, 0.96298; $\delta = \alpha$, 0.98228.

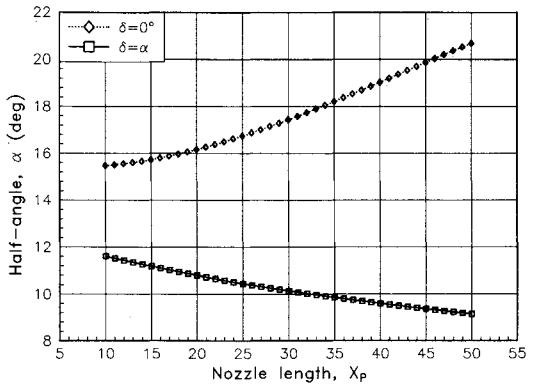

Fig. 5 Optimum half-angle as a function of nozzle length.

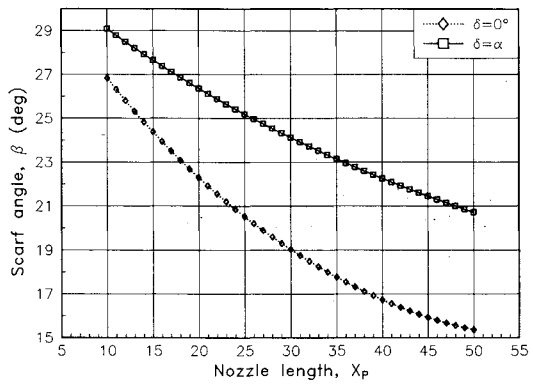

Fig. 6 Optimum scarf angle as a function of nozzle length.

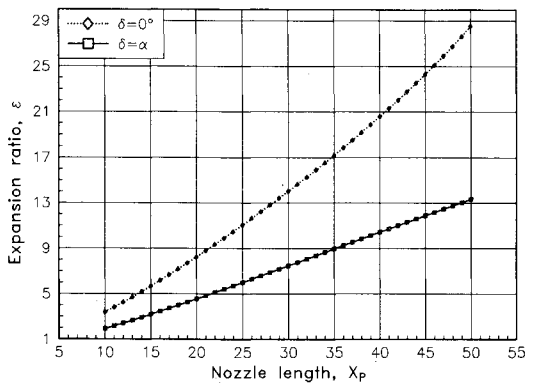

Fig. 7 Optimum expansion ratio as a function of nozzle length.

System Optimization

With the optimum geometries for length-constrained scarfed nozzles determined, a methodology must be established for the incorporation of these nozzle designs as a part of the total propulsion system. The results presented in the preceding section were concerned with scarfed nozzles in general, and were applicable to any type of propulsion system employing scarfed nozzles. The following section, however, is concerned specifically with the design of solid propellant propulsion systems. In particular, emphasis will be placed on fixed-diameter, fixed total impulse, length-constrained, solid propellant systems employing scarfed nozzles. The objective of this part of the investigation is to develop a means of minimizing the overall length of such systems through the proper selection of the scarfed-nozzle design.

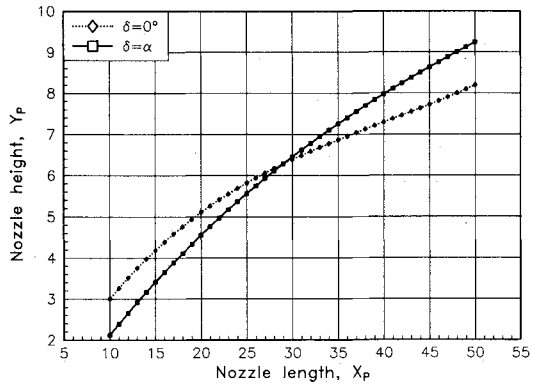

Fig. 8 Optimum nozzle height as a function of nozzle length.

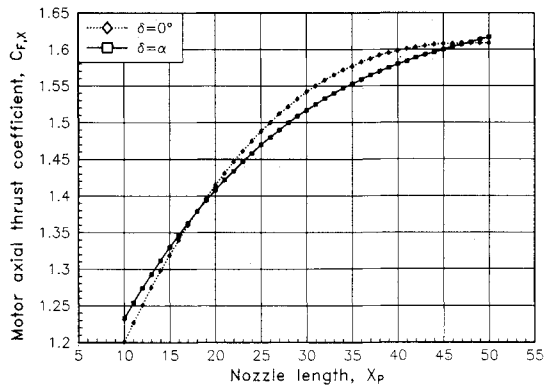

Fig. 9 Optimum motor axial thrust coefficient as a function of nozzle length.

Table 3 Curve-fit coefficients for optimum nozzle geometries

Y	A	B	C	D	E	R^2
			$\delta = 0$ deg			
β	1.0351E−06	−1.5299E−04	1.2939E−02	−7.5016E−01	3.3181E+01	1.00000
α	−6.3739E−08	−3.6963E−05	5.2911E−03	−6.2695E−02	1.5604E+01	0.99999
ϵ	3.4593E−06	−3.7518E−04	1.8543E−02	1.3920E−01	4.7660E−01	0.99999
Y_p	−2.1866E−07	9.3630E−05	−9.1241E−03	4.2108E−01	−3.8453E−01	0.99999
$C_{F,X}$	3.3119E−08	−6.2261E−07	−4.7734E−04	3.5599E−02	8.9318E−01	0.99999
			$\delta = \alpha$			
β	1.9354E−07	−3.5178E−05	4.0081E−03	−3.7049E−01	3.2422E+01	1.00000
α	4.6476E−08	−1.0749E−05	1.2887E−03	−1.1281E−01	1.2616E+01	0.99999
ϵ	8.2820E−07	−1.2538E−04	6.8574E−03	1.3332E−01	1.3704E−02	1.00000
Y_p	−7.4041E−08	3.1526E−05	−4.3413E−03	3.5227E−01	−9.9646E−01	1.00000
$C_{F,X}$	4.1928E−09	2.8719E−06	−5.1337E−04	3.0847E−02	9.7269E−01	0.99999

For the type of propulsion system under consideration, the following set of variables can be used to specify the design requirements:

I_{tot} = total delivered impulse
D = inside diameter of the motor
P_c = operating pressure of the motor
$L_{ps_{max}}$ = maximum allowable system length

In designing such a propulsion system, the first step is to assume a reasonable value for the motor axial specific impulse. This specific impulse will be established as a reference, and is denoted as $I_{sp,X_{ref}}$. Using this reference specific impulse value, a grain design can be obtained to meet the total impulse, operating pressure, and diameter requirements. With reference grain design established, the selection of the optimum nozzle geometry can be used to adjust the length of the propulsion system to produce a minimum-length design. Therefore, the objective of this part of the investigation is to develop a methodology by which the design of this minimum-length system can be obtained. In developing this optimization methodology, two types of solid propellant grains were considered: internal burning grains and end burning grains.

Internal Burning Grains

In designing a motor employing an internal burning grain, the assumption was made that the grain has a cylindrical section with a constant propellant cross-sectional area. Any adjustments to the reference grain design will occur by changing the length of this section. In addition, it is assumed that the following properties will be constant for all of the motor designs considered.

ρ_p = solid propellant density
P_r = perimeter of the burning surface in the cylindrical section
A_{cr} = cross-sectional area of the propellant in the cylindrical section
K_N = initial ratio of burning surface area to throat area

The length of the propellant grain can be expressed as a function of the delivered specific impulse of the rocket motor by the following expression:

$$L_g = L_{g_{ref}} + \Delta L_g \tag{21}$$

where L_g is the length of the grain, $L_{g_{ref}}$ the length of the reference grain, and ΔL_g the increase in grain length due to a change in specific impulse. This value is given by

$$\Delta L_g = [-I_{tot}/(I_{sp,X_{ref}}\rho_p A_{cr})](1 - I_{sp,X_{ref}}/I_{sp,X_{del}}) \tag{22}$$

where $I_{sp,X_{del}}$ is the motor axial specific impulse that will be delivered by the rocket motor. This value is given by

$$I_{sp,X_{del}} = \eta I_{sp,X} \tag{23}$$

where η is the impulse efficiency which must be experimentally obtained, and $I_{sp,X}$ is the motor axial specific impulse as determined from the curve fit for the optimum nozzle performance.

The value for $I_{sp,X}$ is determined from the thrust coefficient value given by

$$C_{F,X} = AX_p^4 + BX_p^3 + CX_p^2 + DX_p + E \tag{24}$$

where the coefficients are obtained from Table 3. The conversion from thrust coefficient to specific impulse is accomplished through manipulation of Eq. (14).

The burning surface area of the grain required for a certain delivered specific impulse value is given by

$$A_b = A_{b_{ref}} + \Delta L_g P_r \tag{25}$$

where A_b is the burning area and $A_{b_{ref}}$ the burning surface area of the reference grain. The radius of one nozzle throat, r_t, can be calculated from the following set of relationships:

$$K_N = A_b/A_t \tag{26}$$

$$A_t = A_b/K_N \tag{27}$$

$$r_t = [A_b/(\pi K_N N_N)]^{1/2} \tag{28}$$

$$r_t = [(A_{b_{ref}} + \Delta L_g P_r)/(\pi N_N K_N)]^{1/2} \tag{29}$$

where N_N is the number of nozzles.

With the throat radius known, the actual projected length of one nozzle is given by

$$L_N = r_t X_p \tag{30}$$

$$L_N = X_p[(A_{b_{ref}} + \Delta L_g P_r)/(\pi N_N K_N)]^{1/2} \tag{31}$$

Therefore, from the relationships presented previously, the specification of the nozzle nondimensional length X_p will determine the grain length and projected nozzle length.

End Burning Grains

The second type of solid propellant grain to be considered is the end burning grain. In optimizing this motor design, the assumption is made that the grain has a constant cross-sectional area. It is also assumed that the following properties will be constant for all motor designs: ρ_p, A_b, P_c, C^*, and t_b, where t_b is the motor burn time. In addition, since the grain is an end burner,

$$A_b = A_{cr} \tag{32}$$

For end burning grains, the length of the grain is determined in the same manner as that presented for internal burning grains. Therefore, Eqs. (21-24) apply.

The constant burn time of the motor is maintained for various changes in grain length by appropriate adjustments in the burning rate. Therefore, the burning rate of the motor is given by

$$r_b = r_{b_{ref}} + \Delta L_g/t_b \tag{33}$$

where r_b is the burning rate, and $r_{b_{ref}}$ is the burning rate of the reference design.

For a solid rocket motor under steady-state operating conditions, the following relationship exists:

$$\rho_p A_b r_b = g A_t P_c/C^* \tag{34}$$

The radius of one throat is, therefore, given by

$$r_t = [\rho_p A_b r_b C^*/(g P_c \pi N_N)]^{1/2} \tag{35}$$

Applying Eq. (33) to Eq. (35) yields

$$r_t = [(\rho_p A_b C^*/(g P_c \pi N_N))(r_{b_{ref}} + \Delta L_g/t_b)]^{1/2} \tag{36}$$

Equation (36) can then be applied to Eq. (30) to obtain the length of a single nozzle.

Motor Dome Nozzle Attachment

There is one more factor influencing the total length of the propulsion system—the length required to attach the nozzles to the rocket motor. Typically, the aft closure of a tactical rocket motor consists of an elliptical dome to which the scarfed nozzles are attached. An illustration of such an arrangement is presented in Fig. 10. The additional distance required by the dome, L_D, is given by the following

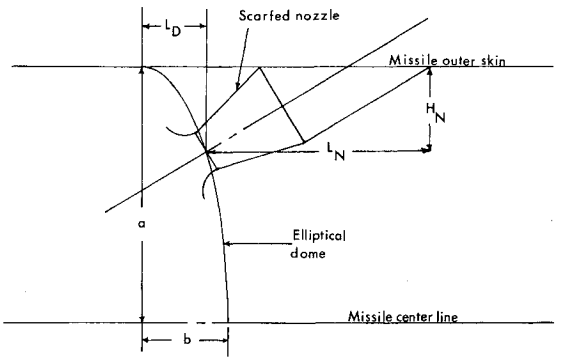

Fig. 10 Dome geometric model.

relationship:

$$L_D = b\left(1 - \frac{1}{a^2}(a - H_N)^2\right)^{1/2} \tag{37}$$

where a is the major radius of the dome and b the minor radius. The projected height of one nozzle, H_N, is given by

$$H_N = r_t Y_p \tag{38}$$

By applying the appropriate relationships in Eq. (37), the value of L_D is expressed as a function of X_p.

Propulsion System Length

The length of the entire propulsion system L_{ps} can be expressed as follows:

$$L_{ps} = L_{g_{ref}} + \Delta L_g(X_p) + L_N(X_p) + L_D(X_p) \tag{39}$$

It is evident that the length of the propulsion system can be expressed solely as a function of X_p. Therefore, the objective is to determine the value of X_p for which L_{ps} is a minimum. This is achieved by satisfying the following equation:

$$\frac{\partial L_{ps}}{\partial X_p} = 0 \tag{40}$$

where

$$\frac{\partial L_{ps}}{\partial X_p} = \frac{\partial L_{g_{ref}}}{\partial X_p} + \frac{\partial \Delta L_g}{\partial X_p} + \frac{\partial L_N}{\partial X_p} + \frac{\partial L_D}{\partial X_p} \tag{41}$$

where, since $L_{g_{ref}}$ is a constant,

$$\frac{\partial L_{g_{ref}}}{\partial X_p} = 0 \tag{42}$$

For an internal burning grain,

$$\frac{\partial \Delta L_g}{\partial X_p} + \frac{\partial L_N}{\partial X_p} = \frac{-I_{tot}}{\rho_p A_{cr}(I_{sp,X_{del}})^2} \frac{\partial I_{sp,X_{del}}}{\partial X_p} \times \left\{1 + \frac{P_r X_p}{2}\left[\frac{1}{N_N \pi K_N}\right]^{1/2}(A_{b_{ref}} + P_r \Delta L_g)^{-1/2}\right\} + \left[\frac{A_{b_{ref}} + P_r \Delta L_g}{N_N \pi K_N}\right]^{1/2} \tag{43}$$

For an end burning grain,

$$\frac{\partial \Delta L_g}{\partial X_p} + \frac{\partial L_N}{\partial X_p} = \frac{-I_{tot}}{\rho_p A_b (I_{sp,X_{del}})^2} \frac{\partial I_{sp,X_{del}}}{\partial X_p} \times \left\{1 + \frac{X_p}{2t_b}\left[\frac{\rho_p A_b C^*}{g P_c \pi N_N}\right]^{1/2}(r_{b_{ref}} + \Delta L_g/t_b)^{-1/2}\right\} + \left[\frac{\rho_p A_b C^*}{g P_c \pi N_N}(r_{b_{ref}} + \Delta L_g/t_b)\right]^{1/2} \tag{44}$$

For all grains

$$\frac{\partial L_D}{\partial X_p} = \frac{b}{a^2} \frac{(a - H_N)}{[1 - 1/a^2(a - H_N)^2]^{1/2}}\left[\frac{\partial Y_p}{\partial X_p} r_t + Y_p \frac{\partial r_t}{\partial X_p}\right] \tag{45}$$

where H_N is given by Eq. (38).

For internal burning grains

$$\frac{\partial r_t}{\partial X_p} = \frac{-I_{tot}}{\rho_p A_{cr}(I_{sp,X_{del}})^2} \frac{P_r}{2}\left[\frac{1}{\pi K_N N_N}\right]^{1/2} \times (A_{b_{ref}} + P_r \Delta L_g)^{-1/2} \frac{\partial I_{sp,X_{del}}}{\partial X_p} \tag{46}$$

where r_t is given in Eq. (29).

For end burning grains

$$\frac{\partial r_t}{\partial X_p} = \frac{-I_{tot}}{\rho_p A_b (I_{sp,X_{del}})^2 2t_b}\left[\frac{\rho_p A_b C^*}{N_N g P_c \pi}\right]^{1/2} \times (r_{b_{ref}} + \Delta L_g/t_b)^{-1/2} \frac{\partial I_{sp,X_{del}}}{\partial X_p} \tag{47}$$

where r_t is given by Eq. (36).

The functional relationships for $C_{F,X}$ and Y_p are given by Eq. (20). Differentiating Eq. (20) with respect to X_p yields

$$\frac{\partial Y}{\partial X_p} = 4AX_p^3 + 3BX_p^2 + 2CX_p + D \tag{48}$$

The preceding relationship can be used to determine the form of

$$\frac{\partial C_{F,X}}{\partial X_p} \quad \text{and} \quad \frac{\partial Y_p}{\partial X_p}$$

by substituting the appropriate coefficients from Table 3.

To convert the expression for $C_{F,X}$ to delivered specific impulse, the following relationship is used:

$$\frac{\partial I_{sp,X_{del}}}{\partial X_p} = \eta \frac{C^*}{g} \frac{\partial C_{F,X}}{\partial X_p} \tag{49}$$

Thus, Eq. (40) can be expressed as

$$\frac{\partial \Delta L_g}{\partial X_p} + \frac{\partial L_N}{\partial X_p} + \frac{\partial L_D}{\partial X_p} = 0 \tag{50}$$

where the appropriate relationships can be substituted for each of the three terms. The solution of this equation will yield the nondimensional nozzle length, which will minimize the overall length of the propulsion system. This optimum value of nozzle length, $X_{p_{opt}}$, can be used to completely determine the optimum nozzle geometry for the set of mis-

sion requirements. Using Eq. (20) and the values in Table 3, the nozzle design parameters can be obtained.

Conclusions

A methodology for the design and optimization of propulsion systems employing scarfed nozzles has been developed. The result of this investigation provides the rocket motor designer with a set of tools with which to analyze and design propulsion systems employing scarfed nozzles. The two-dimensional computer model is an analysis tool which provides the analyst with an accurate performance prediction capability. The curve fits and relationships based on this model provide the designer with a methodology for selecting the appropriate nozzle design. These tools provide a means of producing better scarfed-nozzle designs.

References

[1]Lilley, J. S., "The Design and Optimization of Propulsion Systems Employing Scarfed Nozzles," AIAA Paper 85-1308, July 1985.

[2]Lilley, J. S. and Hoffman, J. D., "Performance Analysis of Scarfed Nozzles," *Journal of Spacecraft and Rockets,* Vol. 23, Jan.-Feb. 1986, pp. 55-62.

[3]Lilley, J. S. and Hoffman, J. D., "The Analysis and Design of Scarfed Nozzles," USAMC TR-RK-85-2, Aug. 1985.

[4]Hoffman, J. D., "A Computer Program for the Performance Analysis of Scarfed Nozzles," USAMC RK-CR-8403, May 1984.